Yao, Y., et al., 2021, Permafrost thaw induced abrupt changes in hydrology and carbon cycling in Lake Wudalianchi, northeastern China: Geology, v. 49, https://doi.org/10.1130/G48891.1

Supplemental Materials

Permafrost thaw induced abrupt changes in hydrology and carbon cycling in Lake Wudalianchi, northeastern China

Yuan Yao [1,2,3,*], Yongsong Huang [2,3,*], Jiaju Zhao [2], Li Wang [4], Youhua Ran [5], Weiguo Liu [2], Hai Cheng [1,2,6]

[1] *Institute of Global Environmental Change, Xi'an Jiaotong University, Xi'an 710054, China*

[2] *State Key Laboratory of Loess and Quaternary Geology, Institute of Earth Environment, Chinese Academy of Sciences, Xi'an 710061, China*

[3] *Department of Earth, Environmental and Planetary Sciences, Brown University, Providence, RI 02912, USA*

[4] *State Key Laboratory of Organic Geochemistry, Guangzhou Institute of Geochemistry, Chinese Academy of Sciences, Guangzhou 510640, China*

[5] *Northwest Institute of Eco-Environment and Resources, Chinese Academy of Sciences, Lanzhou 730000, China*

[6] *Key Laboratory of Karst Dynamics, Ministry of Land and Resources, Institute of Karst Geology, Chinese Academy of Geological Sciences, Guilin 541004, China*

*Corresponding authors:

E-mail address: Y. Yao (yaoyuan@xjtu.edu.cn);

Y. Huang (yongsong_huang@brown.edu)

Supplemental Text

Text S1. Study sites, hydrogeologic background, and samples

Lake Wudalianchi (48°40′N–48°47′N; 126°06′E–126°15′E), the second largest volcanic dammed lake in China, is located near the southern limit of permafrost (SLP) in northeastern China (Figs. 1B and S1). The latest volcanic eruption occurred in 1776 (Laoheishan eruption) (Sun et al., 2019). Meanwhile, lava flows dammed the Shilong River channel, forming five connected lakes (Wudalianchi Pool 1, Pool 2, Pool 3, Pool 4, and Pool 5) of Wudalianchi. There are two river inflows into and one river outflow from Lake Wudalianchi (Figs. 1C, 1D and S2). Due to higher elevations in the north, east, and west of Wudalianchi region, the regional lake water flows southward. Lake Wudalianchi is currently freshwater lake with measured salinity of 0.09‰ in summer of 2016 (Yao et al., 2019a), but annual evaporation (1257 mm) greatly exceeds annual precipitation (468 mm) (Gui et al., 2012). There is massive amounts of groundwater storage in this region (1.7 billion m^3 in Dedu county alone), and the depth of the groundwater table is ~5–30 m in general (Chen, 1994). The groundwater in aquifers can be transported into Shilong River and Lake Wudalianchi (Gui et al., 2012).

We collected an 82-cm sediment core from the center of Lake Wudalianchi Pool 2 with a water depth of ~ 11 m in March of 2018 (Fig. S2). At 65–69 cm depth, the sediments are dominated by dark grey ash deposits, marking the most recent volcanic eruption event in 1776. The core above 69 cm was sub-sampled at 0.5 cm intervals, and the samples below 69 cm were sub-sampled at 1 cm intervals. We focus on the uppermost 69-cm sediments in this study, capturing sediment deposition since the volcanic eruption event in 1776.

The surface sediments (top 0–2 cm) from 10 oligohaline lakes throughout northern China were collected in the summer of 2017 for establishing RIK_{37}-salinity calibration, in combination with our previously published 10 freshwater lakes (Yao et al., 2019b) (Figs. S4 and S5; Table S1). Our calibration has a lower slope than that from the Baltic Sea (Fig. S5), which may result from different salinity tolerance of Group I and Group II Isochrysidales species between lacustrine and estuary marine environments.

Text S2. Chronology

^{210}Pb and ^{137}Cs in the Wudalianchi core were determined by a gamma detector (Ortec). The ^{137}Cs activity peak was detected at 14.5 cm, which corresponds to 1963 (Appleby, 2002) (Fig. S3; Table S2). The age model of our high-resolution sediment core since 1881 (36.5 cm) was constructed using a constant-rate-of-supply (CRS) model (Sanchez-Cabeza and Ruiz-Fernández, 2012) based on ^{210}Pb and using the ^{137}Cs peak as a fixed 1963-yr time marker (Fig. S3; Table S2). From 1776 (65–69 cm; latest volcanic eruption event) to 1881 (36.5 cm), the chronology was established by using a linear interpolation assuming the bottom age of 1776.

Text S3. Sample pretreatment and analysis

For lipid analysis, all sediment samples were freeze-dried and extracted by sonication (3×) with dichloromethane (DCM)/methanol (MeOH) (9:1, v/v). The extracts were purified by column chromatography with silica gel using *n*-hexane, dichloromethane (DCM), and MeOH, respectively. Alkenones in the DCM fractions were analyzed by an Agilent 7890N gas chromatography system equipped with a flame ionization detector (GC-FID) and a Restek Rtx-200 GC column (105 m × 250 μm × 0.25 μm) (Zheng et al., 2017). The following GC-FID oven program was used: initial temperature of 50 °C (hold 2 min), ramp 20 °C /min to 255°C, ramp 3 °C /min to 320 °C (hold 25 min). Diploptene in the hexane fractions was analyzed by gas chromatography-mass spectrometry (GC-MS; Thermo Fisher Scientific), and the $\delta^{13}C$ values were analyzed using a Trace GC Ultra^{TM} (Thermo Scientific) coupled via a combustion reactor to a Delta V Advantage isotope ratio mass spectrometer (Thermo Scientific). The following GC oven program was used: initial temperature of 80 °C (hold 2 min), ramp 3 °C /min to 300 °C (hold 10 min). The $\delta^{13}C$ values are reported relative to the Vienna Pee Dee Belemnite (VPDB) standard ($\delta^{13}C=[(R_{sample}-R_{standard})/R_{standard}]\times1000$; where R is the $^{13}C/^{12}C$ ratio), and the analytical error is ±0.3‰. The reproducibility and accuracy for diploptene carbon isotopes were evaluated by measuring *n*-alkane standards (C_{21}, C_{25}, C_{27}, C_{29}, C_{31}, and C_{33} *n*-alkanes) between every five measured samples. GDGTs in the MeOH fractions were analyzed using high performance liquid chromatography coupled to atmospheric pressure chemical ionization-mass spectrometry (HPLC-APCI-MS) with a Shimadzu LC-MS 8030. GDGTs were eluted with a linear gradient of eluent A (isopropanol) and eluent B (*n*-hexane), decreasing from 97% B to 95% B in 85 min. The column was thereafter cleaned with 90% A for 20 min after each injection. Scanning was performed in selected ion monitoring (SIM) mode to target specific *m*/*z* values for each GDGT compounds (GDGT-0 (1302), GDGT-1 (1300), GDGT-2 (1298), GDGT-3 (1296), crenarchaeol and its regioisomer (1292)), 15 brGDGTs (IIIa (1050), IIIa′ (1050), IIIb

(1048), IIIb′ (1048), IIIc (1046), IIIc′ (1046), IIa (1036), IIa′ (1036), IIb (1034), IIb′ (1034), IIc (1032), IIc′ (1032), Ia (1022), Ib (1020), and Ic (1018)).

The RIK_{37} index (Longo et al., 2016) is calculated as

$$RIK_{37} = \frac{[C_{37:3a}]}{[C_{37:3a} + C_{37:3b}]} \quad (1)$$

where the "*a*" and "*b*" subscripts refer to the $\Delta^{7,14,21}$ and $\Delta^{14,21,28}$ tri-unsaturated alkenones, respectively.

The HP5 index (Yao et al., 2020a) is calculated as

$$HP5 = \frac{IIIa}{IIa+IIIa} \quad (2)$$

Lignin phenols were isolated from the solvent-extracted sediment samples using the alkaline CuO oxidation method (Feng et al., 2011). The samples were reacted with 0.5 g CuO, 100 mg ammonium iron (II) sulfate hexahydrate, and 3 mL of 12 M sodium hydroxide (NaOH) under N_2 at 170°C for 2.5 h. After the reaction, the water phase was acidified to pH 1 with 6 M HCl and kept for 1 h at room temperature in the dark to prevent reactions of cinnamic acids. The lignin oxidation productions were liquid-liquid extracted with ethyl acetate after centrifugation (2500 rpm for 30 min). The lignin phenols were analyzed on a GC-MS (Thermo Fisher Scientific). The following GC oven program was used: initial temperature of 65 °C (hold 2 min), ramp 6 °C /min to 300 °C. Quantification was calculated by a known amount of internal standards (ethyl vanillin) in each sample.

We measured bulk organic carbon and nitrogen isotope ratios using solvent-extracted sediment residuals (i.e., kerogen organics). The sediment samples were treated with 2 M HCl to remove carbonates, and then were rinsed to a pH of ~ 7 with deionized water. A portion of the dried samples were combusted for 4 h at 850 °C in evacuated sealed quartz tubes with 1g CuO, 1g Cu and Pt foil. The CO_2 was then cryogenically purified. The carbon isotopic ratios of the purified CO_2 were measured using a Finnigan MAT 251 gas source mass spectrometer. The $\delta^{13}C$ values were reported relative to the VPDB standard ($\delta^{13}C=[(R_{sample} - R_{standard})/R_{standard}]\times1000$; where R is the $^{13}C/^{12}C$ ratio), and the analytical error is ±0.2‰. The nitrogen isotopic ratios of the samples treated by HCl were determined using a FLASH EA1112 elemental analyzer interfaced with a MAT-Delta-Plus continuous-flow isotope ratio mass spectrometer. The $\delta^{15}N$ values were reported relative to the atmospheric N_2 isotopic standard, and the analytical error is ±0.3‰. The reproducibility and accuracy for bulk carbon and nitrogen isotopes were

evaluated by measuring respectively CO_2 and IAEA-N_3 standards between every five measured samples. The total organic carbon and nitrogen contents of solvent-extracted sediment residuals after removing carbonates with 2 M HCl were measured on a Vario EL III elemental analyzer. The analytical errors are less than ±0.05%.

Text S4. Alkenone isomer-based RIK_{37} as salinity proxy

To reconstruct past hydrological changes in Lake Wudalianchi, we use RIK_{37} index based on the isomeric ratio of tri-unsaturated C_{37} alkenones produced by Group I and/or II Isochrysidales (Longo et al., 2016). From freshwater to oligohaline lakes, salinity serves as the main control for the transition among different groups of alkenone-producing Isochrysidales (Yao et al., 2020): Group I occurs in freshwater/oligohaline lakes (Longo et al., 2016; Yao et al., 2019b), whereas Group II becomes progressively more competitive as salinity increases (Group I rarely occurs in waters with salinity higher than 5‰) (Kaiser et al., 2019; Yao et al., 2020). In the Baltic Sea, for example, as salinity increases from near fresh in Bothnian Bay to brackish waters, Group II Isochrysidales become increasingly more competitive against Group I Isochrysidales (Kaiser et al., 2019). Group I Isochrysidales feature the distinctive alkenone distributions with the presence of isomeric tri-unsaturated C_{37} alkenones with $\Delta^{14,21,28}$ double bond positions ($C_{37:3b}$), in addition to the common $\Delta^{7,14,21}$ ($C_{37:3a}$) in Group II Isochrysidales (Longo et al., 2016; Yao et al., 2019b) (Fig. S8). Based on above rationale, the RIK_{37} index has been proposed as a salinity proxy in freshwater/oligohaline environments (Kaiser et al., 2019), and has been successfully applied for paleosalinity reconstruction in an oligohaline lake of arid central Asia (Yao et al., 2020).

Text S5. Climate Model

We model northward retreat of SLP boundary (0℃ MAAT isotherm) in northeastern China since the 1970s based on a MAAT model (Ran et al., 2018). The potential thermal degradation of permafrost during the 1970s to 2010s was evaluated using MAAT model (Ran et al., 2018). Following the method (Ran et al., 2018), the decadal MAATs (1970–2018) were estimated by integrating the time-series MAAT data from 44 weather stations and remote-sensing-based mean annual land surface temperatures (MASTs), leaf area index (LAI), snow cover duration (SCD), as well as digital elevation model (DEM) data (2000–2010) that represent the pattern of underlying surface, using geographical weighted regression model. A MAAT of 0°C was used to distinguish permafrost from seasonally frozen ground (Jin et al., 2007).

The MAAT data during 1970 to 2018 were obtained from the China Meteorological Administration (http://data.cma.cn). The MAST data were derived from the annual cycle of MODIS land surface temperature product (Bechtel, 2015). The SCD was calculated based on the daily snow cover extent product with 5-km spatial resolution (Hori et al., 2017), and then resampled to 1km, to be consistent with other data. A high-quality LAI product, i.e. the Global Land Surface Satellite (GLASS) with a 1 km spatial resolution (Xiao et al., 2014), is used in this study.

Text S6. Meteorological data

The Harbin weather station recorded the longest MAAT (since 1881) and MAP (since 1909) data in China (Zhang et al., 2011). The station was established in 1898, but a small fraction of MAAT data was missing due to historical reasons. The specialist from meteorological agency in Heilongjiang province made up the missing data by interpolation and comparison with the temperature data from Vladivostok in Russia, and then extended the data to 1881(Zhang et al., 2011). However, the precipitation data between 1943 and 1948 are still missing at present.

Text S7. Lignin biomarkers as traces of permafrost thaw

In the permafrost soils of northern Siberia (Rodionow et al., 2006) and the Tibetan Plateau (Chen et al., 2016), Vd/Vl values (ratio of vanillic acid to vanillin) are higher in the active layer than permafrost deposits, indicating enhanced lignin degradation as permafrost thaws. The index has been successfully applied for tracing permafrost organic carbon mobilization to rivers and coasts in an Alaskan permafrost region (Zhang et al., 2017).

Text S8. Estimating contribution of methanotrophic bacteria to diploptene

We estimated the contributions of methanotrophic bacteria to diploptene using a carbon isotopic mass balance equation (Naeher et al., 2014).

$$f_{\text{methano}} = \frac{\delta^{13}C_{\text{dip-sample}} - \delta^{13}C_{\text{non-CH4}}}{\delta^{13}C_{\text{methano-dip}} - \delta^{13}C_{\text{non-CH4}}} \times 100 \quad (3)$$

Where f_{methano} is the fraction of diploptene produced by methanotrophic bacteria (%). $\delta^{13}C_{\text{dip-sample}}$ is the measured carbon isotopic ratios of diploptene in a given sample. $\delta^{13}C_{\text{non-CH4}}$ is the carbon isotopic ratios of non-CH_4 carbon-derived organic

matter. $\delta^{13}C_{methano\text{-}dip}$ is the assumed carbon isotopic ratios of dioloptene produced by methanotrophic bacteria.

For non-CH_4 carbon-derived organic matter, we used a $\delta^{13}C$ value of -30‰, representing organic carbon from Calvin-Benson-Bassham cycle (CBB) (Lamb et al., 2006). For methanotrophic bacteria, $\delta^{13}C_{methano\text{-}dip}$ was calculated from CH_4 $\delta^{13}C$ value minus the carbon isotopic fractionation during diploptene biosynthesis ($\triangle^{13}C_{biosynthesis}$). CH_4 in permafrost-affected environments is primarily produced by acetate fermentation (McCalley et al., 2014). Overall, the microbial CH_4 from acetate fermentation have relatively constant $\delta^{13}C$ values (McCalley et al., 2014). Because there are no reported $\delta^{13}C$ values of CH_4 from permafrost-affected lakes of our study region, so we used available $\delta^{13}C$ values (-68‰±5‰) of CH_4 bubbles from permafrost-affected Arctic lakes as a representative (Walter Anthony et al., 2016). The $\triangle^{13}C_{biosynthesis}$ values (Jahnke et al., 1999; Templeton et al., 2006) vary from 3‰ to 39‰. Thus, the minimum and maximum of $\delta^{13}C_{methano\text{-}dip}$ are -71‰ and -107‰, respectively. We calculated $f_{methano}$ range using the minimum and maximum of the $\delta^{13}C_{methano\text{-}dip}$.

Text S9. Comprehension of bulk nitrogen isotopes

The positive $\delta^{15}N$ excursion after 1982trend (Fig. 3J) may have been caused by: 1) enhanced denitrification due to warming-induced increase in lake water stratification during the summer and decrease in bottom water redox potential (Lehmann et al., 2003); 2) increased lake primary productivity and more complete nitrogen utilization with the addition of nutrients from decomposing permafrost soils (Davidson et al., 2013). Because the lake does not become anoxic after permafrost thawing, as indicated our HP5 index as a redox proxy (Fig. 3I), the observed positive $\delta^{15}N$ excursion may mainly reflect the increased lake primary productivity. Total organic carbon and nitrogen contents of the sediments also start to rise around 1975 (Figs. 3K, S7C and S7D), which is also consistent with an increase in lake primary productivity. The increase in primary productivity since ~1975 in Lake Wudalianchi did not lead to the commonly observed increase in bulk organic $\delta^{13}C$ values due to CO_2 limitation (Davidson et al., 2013), but in fact quite the contrary (Figs. 3J and S7A). Therefore, the negative $\delta^{13}C$ excursion since ~1975 results from enhanced input of permafrost thaw derived ^{13}C-depleted carbon fluxes and strengthening of the CH_4 cycles.

Supplementary Figures (S1 to S8)

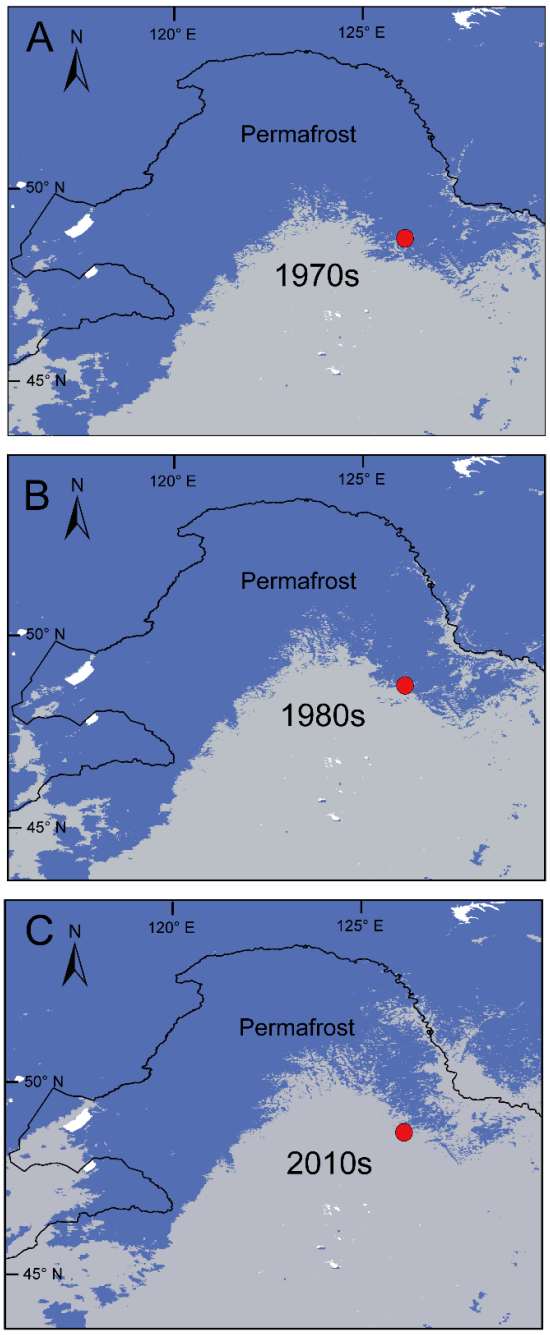

Figure S1. The SLP changes in northeastern China in 1970s, 1980s, 2010s, which were evaluated based on a MAAT model (Ran et al., 2018) by integrating the MAAT data and remote-sensing-based mean annual land surface temperatures (MASTs), leaf area index (LAI), snow cover duration (SCD), as well as digital elevation model (DEM) data that represent the pattern of underlying surface, using geographical weighted regression model (Ran et al., 2018).

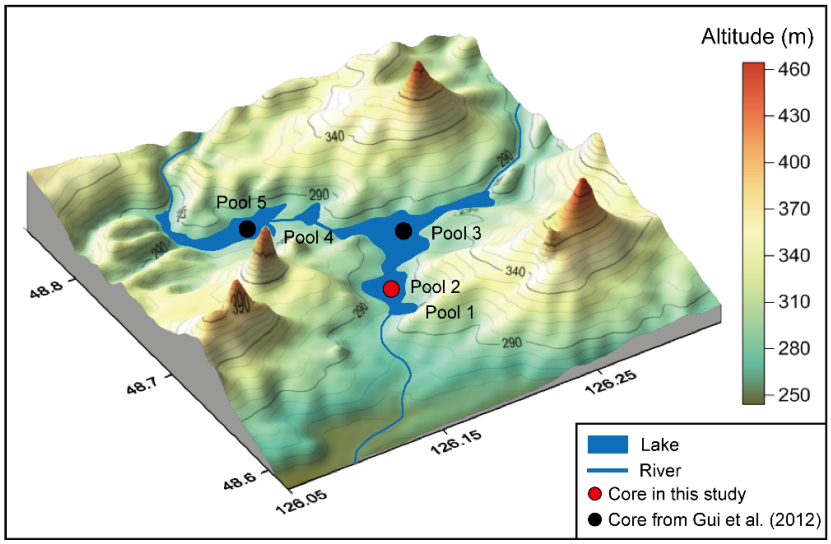

Figure S2. Geographical map of Wudalianchi region with our sediment core (red circle) and published two sediment core sites (Gui et al., 2012) (black circles) as well as surface hydrogeology.

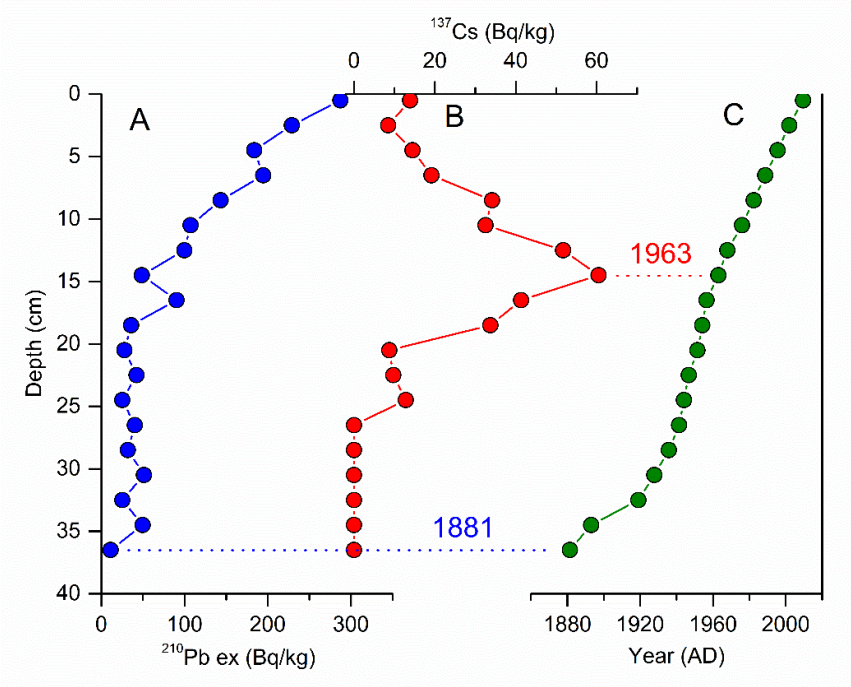

Figure S3. Age model for the Wudalianchi core: (A) ^{210}Pb ex, (B) ^{137}Cs activity, and (C) age-depth relation based on ^{210}Pb and ^{137}Cs dating. The age model was constructed using a constant-rate-of-supply (CRS) model (Sanchez-Cabeza and Ruiz-Fernández) based on ^{210}Pb and using the ^{137}Cs peak as a fixed 1963-yr time marker (Appleby, 2002).

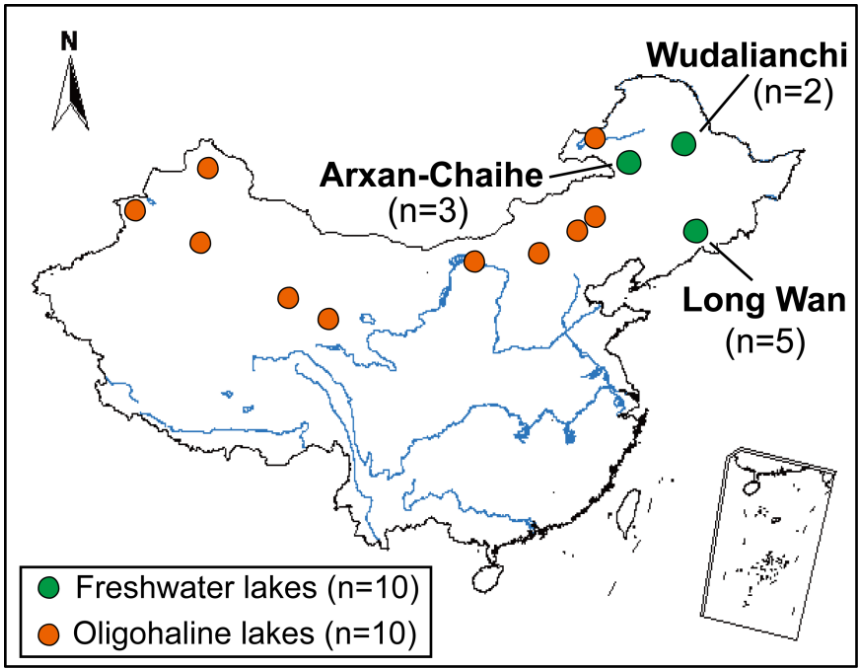

Figure S4. Map showing the geographic locations of surface sediment study sites, including10 freshwater (Yao et al., 2019b) (salinity: < 0.5‰) and 10 oligohaline lakes (salinity: 0.5–5‰) from northern China in this study.

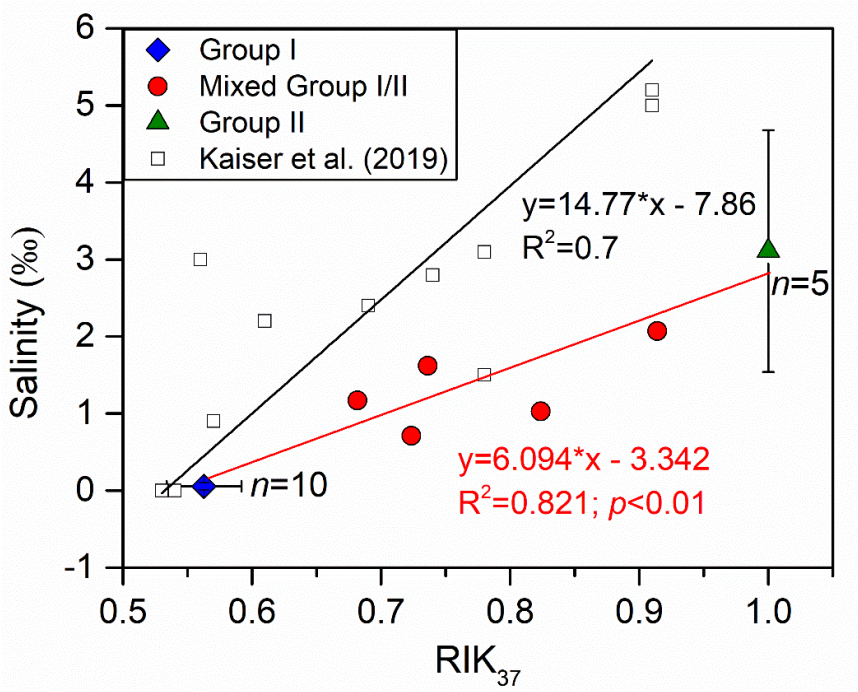

Figure S5. RIK_{37}-salinity calibrations from our study (red line) and the Baltic Sea (Kaiser et al., 2019) (blue line). Our calibration is based on surface sediments from 10 freshwater (Longo et al., 2016) (salinity: < 0.5‰) and 10 oligohaline lakes (salinity: 0.5–5‰) from northern China. The RIK_{37} values of 0.51–0.6 indicate dominated Group I Isochrysidales producer; RIK_{37} values of 0.6–1 indicate the mixture of Group I and Group II Isochrysidales producer; RIK_{37} values of 1 indicate Group II Isochrysidales producer (Longo et al., 2016). Applying the calibration from the Baltic Sea (Kaiser et al., 2019) to our Wudalianchi downcore data would increase the range of inferred salinity changes from 1975 to 1982 by 2.4‰ (rate of 0.34‰ per year), but does change our interpretation of abrupt salinity change resulting from permafrost thaw.

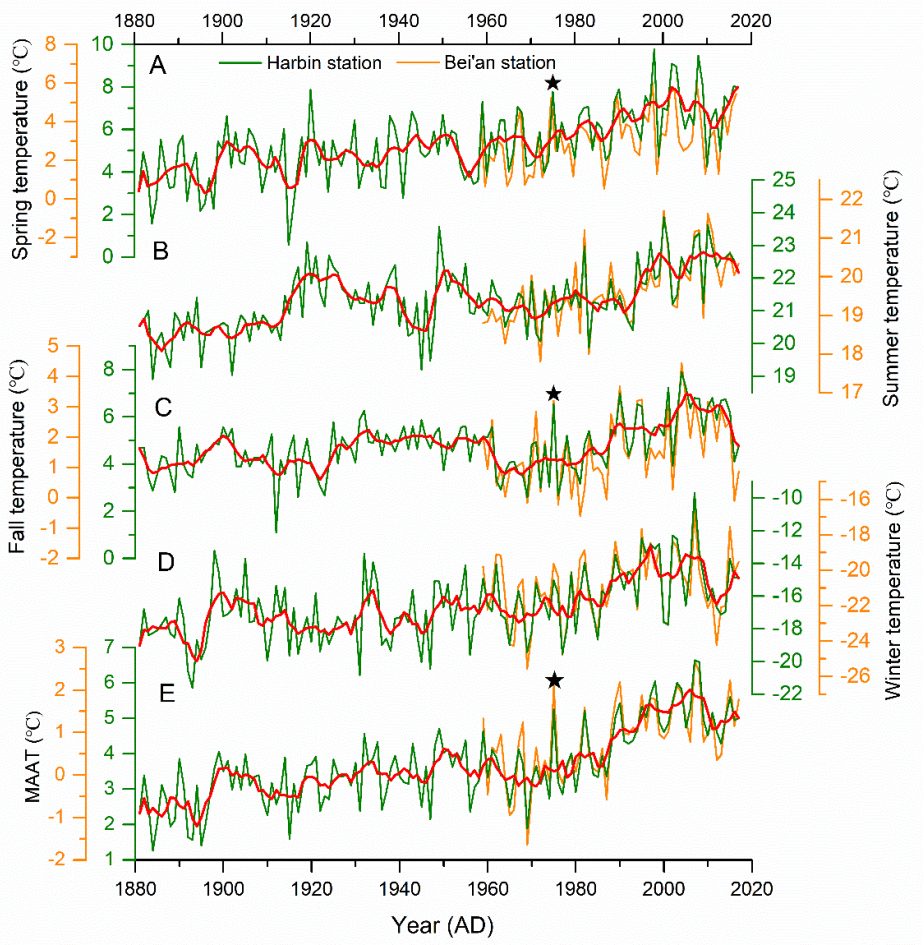

Figure S6. Instrumental mean spring, summer, fall, and winter temperatures, as well as mean annual air temperature (MAAT) of Harbin and Bei'an weather stations (red lines represent 5-point running means for Harbin station). Black stars represent the exceptionally high spring and fall temperatures as well as MAAT in 1975.

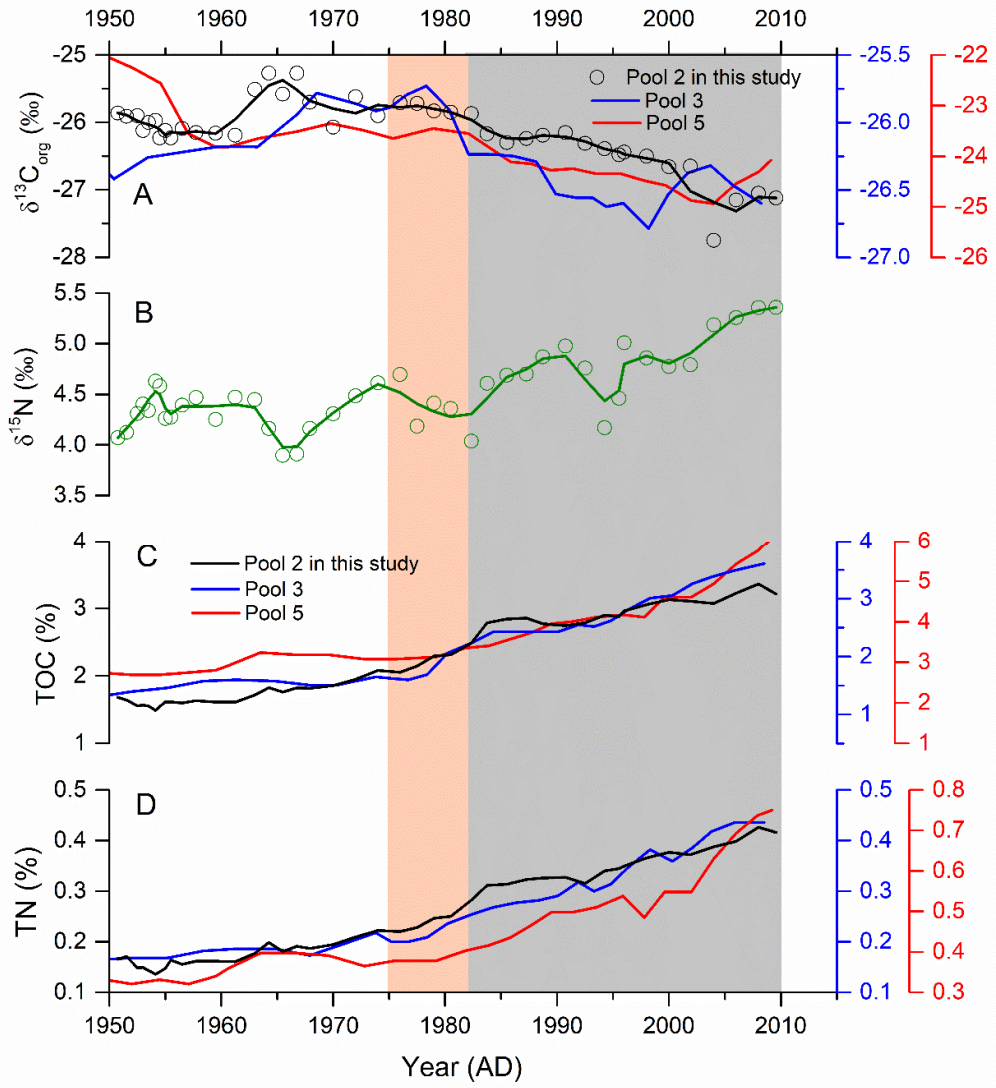

Figure S7. (A) $\delta^{13}C$ values of bulk organic matter in our study Pool 2 (2-point running means) as well as published Pool 3 and Pool 5 (Gui et al., 2012). (B) Bulk $\delta^{15}N$ values in our study Pool 2 (2-point running means). (C) total organic carbon (TOC) and (D) total nitrogen (TN) from our study Pool 2 as well as published Pool 3 and Pool 5 (Gui et al., 2012). Orange shaded area represents the age range from 1975 to 1982; Gray shaded area represents the age from 1982 to 2010.

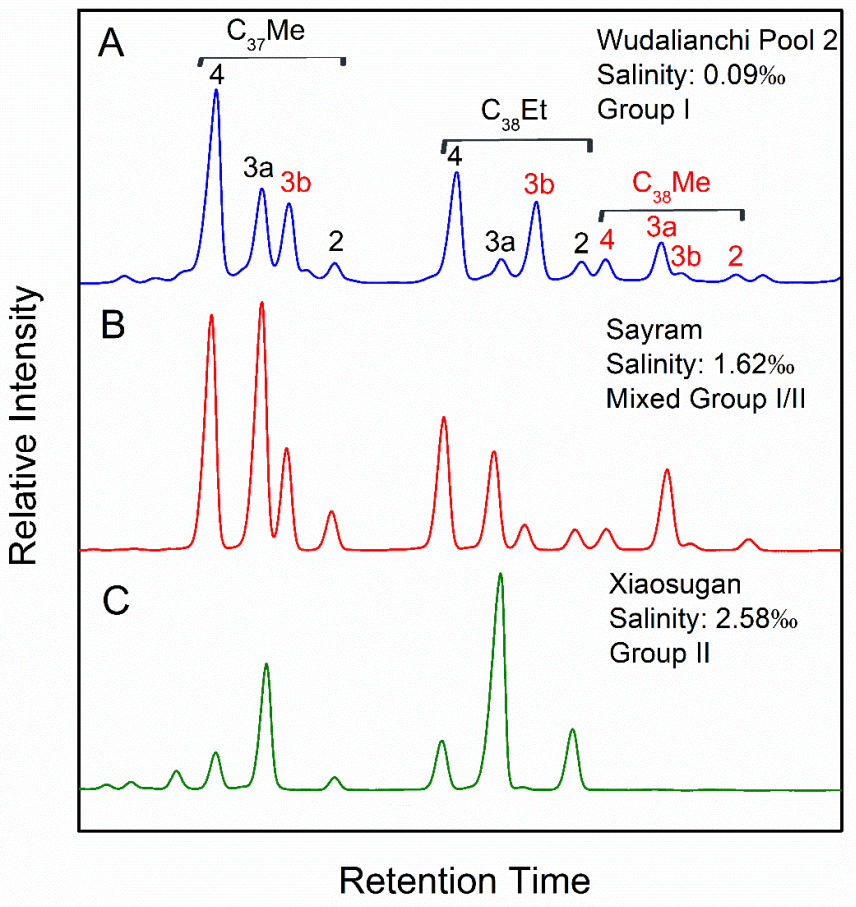

Figure S8. Partial gas chromatograms of long-chain alkenones from Wudalianchi, Wuliangsuhai, and Xiaosugan. Group I Isochrysidales are characterized by the generally equal abundances of $C_{37:3a}$Me and $C_{37:3b}$Me. Group II Isochrysidales do not produce the $C_{37:3b}$Me (Long et al., 2016).

Supplemental Tables (S1 and S2)

Table S1 Location, salinity, and abundances (%) of individual long-chain alkenones in 10 investigated oligohaline lakes from the northern China.

Lakes	Latitude	Longitude	Salinity (‰)	RIK_{37}	C37:4	C37:3a	C37:3b	C37:2	C38:4Et	C38:3aEt	C38:3bEt	C38:2Et	C38:4Me	C38:3aMe	C38:3bMe	C38:2Me
Wuliangsuhai	40.902	108.822	2.07	0.91	12.4	34.8	3.3	7.2	6.0	23.8	1.4	10.0	0.0	1.1	0.0	0.0
Aolunnarisi	43.248	116.419	0.71	0.72	31.4	22.8	8.7	3.1	9.5	8.2	8.8	1.7	2.1	2.9	0.8	0.0
Wulungu	47.262	87.504	1.17	0.68	30.4	17.6	8.2	2.2	14.4	7.7	6.6	0.7	3.7	6.9	0.7	0.9
Sayram	44.632	81.122	1.62	0.74	23.1	25.0	9.0	3.7	13.3	9.9	2.4	2.1	2.2	7.9	0.4	1.2
Bositeng	41.990	86.979	1.03	0.82	16.4	29.5	6.3	3.6	11.4	21.8	2.0	1.0	1.3	5.8	0.0	0.8
Yueya	49.373	117.658	3.66	1	51.2	17.1	0.0	5.5	10.4	15.2	0.0	0.0	0.0	0.0	0.0	0.0
Xiaosugan	39.064	94.220	2.58	1	6.2	23.3	0.0	2.3	9.2	47.4	0.0	11.6	0.0	0.0	0.0	0.0
Xiarinaoer	42.622	115.482	4.97	1	12.3	20.1	0.0	2.3	13.8	40.9	0.4	10.2	0.0	0.0	0.0	0.0
Tianshigou	41.521	113.525	3.59	1	31.3	24.9	0.0	6.6	5.3	21.9	0.0	9.9	0.0	0.0	0.0	0.0
Keluke	37.283	96.893	0.75	1	19.8	23.7	0.0	2.4	19.1	25.2	1.0	8.8	0.0	0.0	0.0	0.0

Table S2 ^{210}Pb and ^{137}Cs data from the sediment core of Lake Wudalianchi.

Lab. No.	Sample No.	Depth (cm)	^{210}Pb ex (Bq/kg)	^{137}Cs (Bq/kg)	Age CRS (AD)
LPR-1808-003	WDLC18-2-0.5	0.5	287	14	2010
LPR-1808-004	WDLC18-2-2.5	2.5	229	8	2002
LPR-1808-024	WDLC18-2-4.5	4.5	184	14	1996
LPR-1808-029	WDLC18-2-6.5	6.5	194	19	1989
LPR-1808-030	WDLC18-2-8.5	8.5	143	34	1982
LPR-1808-031	WDLC18-2-10.5	10.5	107	33	1976
LPR-1808-025	WDLC18-2-12.5	12.5	100	52	1968
LPR-1808-026	WDLC18-2-14.5	14.5	49	60	1963
LPR-1808-027	WDLC18-2-16.5	16.5	90	41	1956
LPR-1808-028	WDLC18-2-18.5	18.5	36	34	1954
LPR-1808-014	WDLC18-2-20.5	20.5	28	9	1952
LPR-1808-015	WDLC18-2-22.5	22.5	42	10	1947
LPR-1808-016	WDLC18-2-24.5	24.5	25	13	1944
LPR-1808-017	WDLC18-2-26.5	26.5	40	0	1941
LPR-1808-018	WDLC18-2-28.5	28.5	32	0	1936
LPR-1808-019	WDLC18-2-30.5	30.5	51	0	1928
LPR-1808-020	WDLC18-2-32.5	32.5	25	0	1919
LPR-1808-021	WDLC18-2-34.5	34.5	50	0	1893
LPR-1808-022	WDLC18-2-36.5	36.5	11	0	1881

Supplemental References

Appleby, P. G., 2002, Chronostratigraphic techniques in recent sediments. In: Tracking Environmental Change Using Lake Sediments: Springer, pp.171–203.

Bechtel, B., 2015, A new global climatology of annual land surface temperature: Remote Sensing, V. 7, P. 2850–2870.

Chen, L., Liang, J., Qin, S., Liu, L., Fang, K., Xu, Y., Ding, J., Li, F., et al., 2016, Determinants of carbon release from the active layer and permafrost deposits on the Tibetan Plateau: Nature Communications, v. 7, p. 13046, doi:10.1038/ncomms13046.

Davidson, T.A., and Jeppesen, E., 2013, The role of palaeolimnology in assessing eutrophication and its impact on lakes: Journal of Paleolimnology, v. 49, p. 391–410, doi:10.1007/s10933-012-9651-0.

Feng, X., Hills, K.M., Simpson, A.J., Whalen, J.K., and Simpson, M.J., 2011, The role of biodegradation and photooxidation in the transformation of terrigenous organic matter: Organic Geochemistry, v. 42, p. 262–274.

Gui, Z., Xue, B., Yao, S., Zhang, F., and Yi, S., 2012, Catchment erosion and trophic status changes over the past century as recorded in sediments from Wudalianchi Lake, the northernmost volcanic lake in China: Quaternary International, v. 282, p. 163–170.

Hori, M., Sugiura, K., Kobayashi, K., Aoki, T., Tanikawa, T., Kuchiki, K., Niwano, M., and Enomoto, H., 2017, A 38-year (1978–2015) Northern Hemisphere daily snow cover extent product derived using consistent objective criteria from satellite-borne optical sensors: Remote sensing of environment, v. 191, p. 402–418.

Jahnke, L.L., Summons, R.E., Hope, J.M., and Des Marais, D.J., 1999, Carbon isotopic fractionation in lipids from methanotrophic bacteria II: the effects of physiology and environmental parameters on the biosynthesis and isotopic signatures of biomarkers: Geochimica et Cosmochimica Acta, v. 63, p. 79–93.

Jin, H., Yu, Q., Lu, L., Guo, D., He, R., Yu, S., Sun, G., and Li, Y., 2007, Degradation of permafrost in the Xing'anling mountains, northeastern China: Permafrost and Periglacial Processes, v. 18, p. 245–258.

Kaiser, J., Wang, K.J., Rott, D., Li, G., Zheng, Y., Amaral-Zettler, L., Arz, H.W., and Huang, Y., 2019, Changes in long chain alkenone distributions and Isochrysidales groups along the Baltic Sea salinity gradient: Organic Geochemistry, v. 127, p. 92–103.

Lamb, A.L. Wilson, G.P. and Leng, M.J., 2006, A review of coastal palaeoclimate and relative sea-level reconstructions using $\delta^{13}C$ and C/N ratios in organic material: Earth-Science Reviews, v. 75, p. 29–57.

Lehmann, M.F., Reichert, P., Bernasconi, S.M., Barbieri, A., and McKenzie, J.A., 2003, Modelling nitrogen and oxygen isotope fractionation during denitrification in a lacustrine redox-transition zone: Geochimica et Cosmochimica Acta, v. 67, p. 2529–2542, doi:10.1016/S0016-7037(03)00085-1.

Longo, W.M., Theroux, S., Gibin, A.E., Zheng, Y., Dillon, J. T., and Huang, Y., 2016, Temperature calibration and phylogenetically distinct distributions for freshwater alkenones: Evidence from northern Alaskan lakes: Geochimica et Cosmochimica Acta, v. 180, p. 177–196.

McCalley, C.K., Woodcroft, B.J., Hodgkins, S.B., Wehr, R.A., Kim, E., Mondav, R., Crill, P.M., Chanton, J.P., Rich, V.I., Tyson, G.W., Saleska, S.R., 2014, Methane dynamics regulated by microbial community response to permafrost thaw: Nature, v. 514, 478–481.

Naeher, S., Niemann, H., Peterse, F., Smittenberg, R.H., Zigah, P.K., and Schubert, C.J., 2014, Tracing the methane cycle with lipid biomarkers in Lake Rotsee (Switzerland): Organic Geochemistry, v. 66, p. 174–181.

Ran, Y., Li, X., and Cheng, G., 2018, Climate warming over the past half century has led to thermal degradation of permafrost on the Qinghai-Tibet Plateau: The Cryosphere, v. 12, p. 595–608.

Rodionow, A., Flessa, H., Kazansky, O., and Guggenberger G., 2006, Organic matter composition and potential trace gas production of permafrost soils in the forest tundra in northern Siberia: Geoderma, v. 135, p. 49-62, doi:10.1016/j.geoderma.2005.10.008.

Sanchez-Cabeza, J.A., and Ruiz-Fernández, A.C., 2012, ^{210}Pb sediment radiochronology: an integrated formulation and classification of dating models: Geochimica et Cosmochimica Acta, v. 82, p. 183–200.

Sun, C., Németh, K., Zhan, T., You, H., Chu, G., and Liu, J., 2019, Tephra evidence for the most recent eruption of Laoheishan volcano, Wudalianchi volcanic field, northeast China: Journal of Volcanology and Geothermal Research, v. 383, p. 103–111.

Templeton, A.S., Chu, K.H., Alvarez-Cohen, L., and Conrad, M.E., 2006, Variable carbon isotope fractionation expressed by aerobic CH_4-oxidizing bacteria: Geochimica et Cosmochimica Acta, v. 70, p. 1739–1752.

Walter Anthony, K., Daanen, R., Anthony, P., Schneider von Deimling, T., Ping, C.-L, Chanton, J.P., and Grosse, G., 2016, Methane emissions proportional to permafrost carbon thawed in Arctic lakes since the 1950s: Nature Geoscience, v. 9, p. 679–682.

Xiao, Z., Liang, S., Wang, J., Chen, P., Yin, X., Zhang, L., and Song, J., 2014, Use of general regression neural networks for generating the GLASS leaf area index

product from time-series MODIS surface reflectance: IEEE Transactions on Geoscience and Remote Sensing, v. 52, p. 209–223.

Yao, Y., Zhao, J., Bauersachs, T., and Huang, Y., 2019a, Effect of water depth on the TEX_{86} proxy in volcanic lakes of northeastern China: Organic Geochemistry, v. 129, p. 88–98.

Yao, Y., Zhao, J., Longo, W.M., Li, G., Wang, X., Vachula, R.S., Wang, K.J., and Huang, Y., 2019b, New insights into environmental controls on the occurrence and abundance of Group I alkenones and their paleoclimate applications: Evidence from volcanic lakes of northeastern China: Earth and Planetary Science Letters, v. 527, p. 115792.

Yao, Y., Zhao, J., Vachula, R.S., Werne, J.P., Wu, J., Song, X., Huang, Y., 2020a, Correlation between the ratio of 5-methyl hexamethylated to pentamethylated branched GDGTs (HP5) and water depth reflects redox variations in stratified lakes: Organic Geochemistry, v. 147, p. 104076, doi:10.1016/j.orggeochem.2020.104076.

Yao, Y., Lan, J., Zhao, J., Vachula, R.S., Xu, H., Cai, Y., Cheng, H., and Huang, Y., 2020b, Abrupt freshening since the early Little Ice Age in Lake Sayram of arid central Asia inferred from an alkenone isomer proxy: Geophysical Research Letters, v. 47, p. e2020GL089257, doi:10.1029/2020GL089257.

Zhang, X. Chen, L., Ji, J., Wang, J., Wang, Y., Guo, W., and Lan, B., 2011, Climate change and its effect in Harbin from 1881 to 2010: Journal of Meteorology and Environment, v. 27, p. 13–20. (in Chinese with English abstract)

Zhang, X., Bianchi, T.S., Cui, X., Rosenheim, B.E., Ping, C-L., Hanna, A.J.M., Kanevskiy, M. Schreiner, K.M., et al., 2017, Permafrost organic carbon mobilization from the watershed to the Colville River Delta: evidence from 14C ramped pyrolysis and lignin biomarkers: Geophysical Research Letters, v. 44, p. 11491–11500, doi:10.1002/2017GL075543.

Zhang, Y.G., Zhang, C.L., Liu, X.-L, Li, Li., Hinrich, K.-U, and Noakes, J.E., 2011, Methane Index: A tetraether archaeal lipid biomarker indicator for detecting the instability of marine gas hydrates: Earth and Planetary Science Letters, v. 307, p. 525–534.

Zheng, Y., Tarozo, R., and Huang, Y., 2017, Optimizing chromatographic resolution for simultaneous quantification of long chain alkenones, alkenoates and their double bond positional isomers: Organic Geochemistry, v. 111, p. 136–143.